Glucose Biosensor from Covalent Immobilization of Chitosan-Coupled Carbon Nanotubes on Polyaniline-Modified Gold Electrode

Dong Wan,[†,‡] Shaojun Yuan,[§,‡] G. L. Li,[†] K. G. Neoh,[†] and E. T. Kang*[,†]

Department of Chemical and Biomolecular Engineering, National University of Singapore, 10 Kent Ridge Crescent, Singapore 119260, and College of Chemical Engineering, Sichuan University, Chengdu, 610065, China

ABSTRACT An amperometric glucose biosensor was prepared using polyaniline (PANI) and chitosan-coupled carbon nanotubes (CS-CNTs) as the signal amplifiers and glucose oxidase (GOD) as the glucose detector on a gold electrode (the Au-*g*-PANI-*c*-(CS-CNTs)-GOD biosensor). The PANI layer was prepared via oxidative graft polymerization of aniline from the gold electrode surface premodified by self-assembled monolayer of 4-aminothiophenol. CS-CNTs were covalently coupled to the PANI-modified gold substrate using glutaradehyde as a bifunctional linker. GOD was then covalently bonded to the pendant hydroxyl groups of chitosan using 1,4-carbonyldiimidazole as the bifunctional linker. The surface functionalization processes were ascertained by X-ray photoelectron spectroscopy (XPS) analyses. The field emission scanning electron microscopy (FESEM) images of the Au-*g*-PANI-*c*-(CS-CNTs) electrode revealed the formation of a three-dimensional surface network structure. The electrode could thus provide a more spatially biocompatible microenvironment to enhance the amount and biocatalytic activity of the immobilized enzyme and to better mediate the electron transfer. The resulting Au-*g*-PANI-*c*-(CS-CNTs)-GOD biosensor exhibited a linear response to glucose in the concentration range of 1−20 mM, good sensitivity (21 μA/(mM · cm^2)), good reproducibility, and retention of >80% of the initial response current after 2 months of storage.

KEYWORDS: glucose biosensor • polyaniline • chitosan • carbon nanotubes • Au electrode

INTRODUCTION

Diabetes is a worldwide public health problem. Its diagnosis and management require tight monitoring of blood glucose levels (1, 2). Electrochemical biosensors, especially amperometric biosensors, for glucose play a leading role in this monitoring process (3−5). Conducting polymers have attracted much attention in the development of efficient amperometric glucose biosensors (6−10). Their unique electroactive properties allow them to act as excellent substrates for the immobilization of biomolecules and rapid transfer of electrons (11, 12). Among the various conducting polymers, polyaniline (PANI) is particularly attractive (13, 14) owing to its high electrical conductivity, ease of preparation and good environmental stability. In biosensor applications, PANI provides a suitable matrix for the immobilization of biomolecules and can significantly improve signal amplification by acting as a mediator for electron transfer in enzymatic reaction (15−18).

In the fabrication of biosensors, chitosan (CS) has been widely used for the immobilization of various enzymes in recent years (19−21). The unusual combination of its properties, such as excellent membrane-forming ability, good adhesion, high mechanical strength, good biocompatibility, and susceptibility to chemical modification arising from the presence of reactive amino and hydroxyl functional groups, has promoted its application in biosensors (22, 23). However, CS is nonconductive, which hampers electron transfer in the biocatalytic process of enzymes (24). On the other hand, functionalization of carbon nanotubes (CNTs) with biomolecules is often a key step in their biological applications, such as biosensing (25). Thus, CS is usually used in combination with conducting polymers, CNTs, redox mediators or metal nanoparticles in electrochemical biosensing platforms (26, 27). Arising from the attractive electronic, chemical and mechanical properties of CNTs, CS/CNTs composites have been explored for the development of electrochemical biosensors (27−29). It is desirable to covalently couple CS with CNTs (CS-CNTs), because CNTs can enhance the conductivity of CS while CS can improve the hydrophilicity and biocompatibility of CNTs, resulting in good dispersity and long-term stability of CS-CNTs in diluted organic acids (30).

Fine amperometric biosensors have been prepared by blending, physical entrapment, layer-by-layer coating, sol−gel reaction and electrochemical deposition of electroactive materials on the surface of electrodes (29, 30, 32−35). To enhance the lifetime stability of enzymatic electrode, it is also of interest to immobilize the enzymes and biomolecules

* To whom all correspondence should be addressed. Tel: +65-6516-2189. Fax: +65-6779-1936. E-mail: cheket@nus.edu.sg.

Received for review July 7, 2010 and accepted October 6, 2010

[†] National University of Singapore.

[‡] These two authors contributed equally.

[§] Sichuan University.

DOI: 10.1021/am100591t

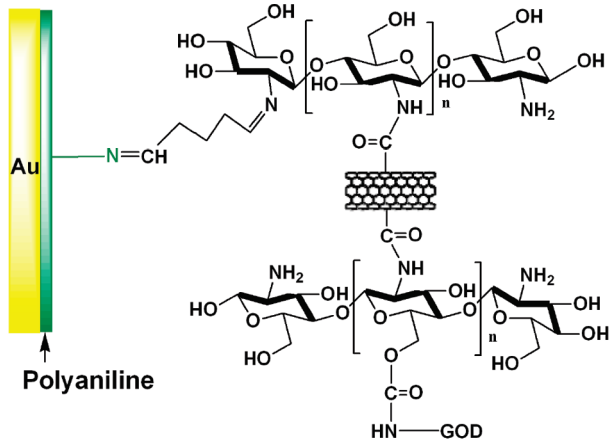

Scheme 1

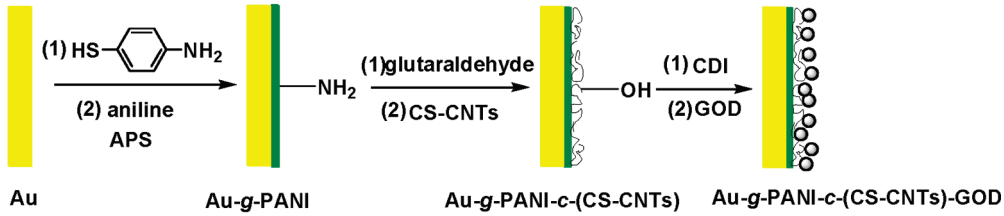

Scheme 2

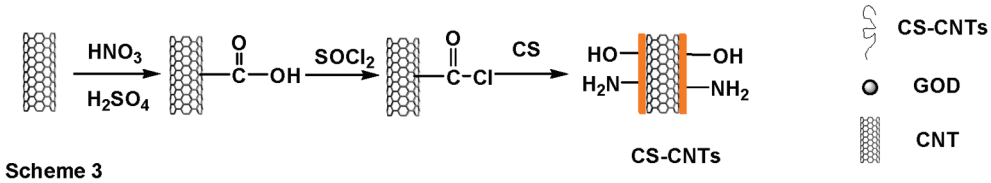

Scheme 3

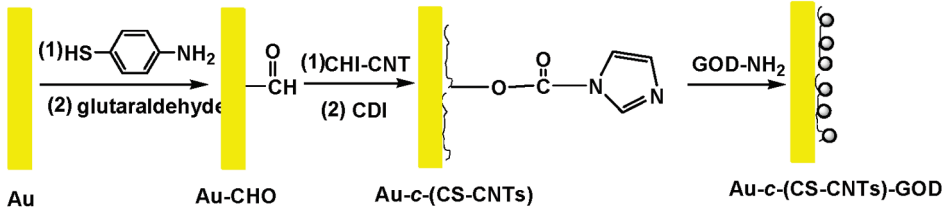

Scheme 4

FIGURE 1. Schematic diagrams illustrating the process of fabrication of the Au-*g*-PANI-*c*-(CS-CNTs)-GOD (Schemes 1−3), and Au-*c*-(CS-CNTs)-GOD (Scheme 4) biosensors.

on electrodes via robust covalent bonds (10, 36, 37). In this work, a gold electrode was first modified by oxidative graft polymerization of aniline, followed by covalent immobilization of the CS-CNTs composites via glutaraldehyde bifunctional linkers. Carbonyldiimidazole, as a peptide coupling agent, was subsequently used to covalently immobilize glucose oxidase on the modified gold electrode. Schemes 1−3 in Figure 1 illustrate the procedures for fabricating the amperometric glucose biosensor with covalently bonded surface functionalities.

MATERIALS AND METHODS

Materials. Aniline (99%), 4-aminothiophenol (97%), 1,4-carbonyldiimidazole (97%), glucose oxidase, D(+)-glucose (99.5%). and chitosan (CS, low molecular weight) were obtained from Sigma-Aldrich Chemical Co. Multiwalled carbon nanotubes (MWCNT) were purchased from NanoLab, Inc. Solvents, such as tetrahydrofuran (THF), *N*,*N*′-dimethylformamide (DMF) and dimethyl sulfoxide (DMSO) were of reagent grade and were used as received. Other reagents were used as received. Phosphate buffer solution (PBS) was prepared afresh before use.

Preparation of Chitosan-Coupled Carbon Nanotubes (CS-CNTs). CS-CNTs were synthesized according to the method described in the literature (30) (Scheme 3, Figure 1). The carboxyl-functionalized CNTs (CNTs-COOH) were prepared via sonication in a 1:3 (*v*/*v*) mixture of concentrated nitric/sulfuric acid at 50 °C for 6 h. The acryl chloride-functionalized CNTs (CNTs-COCl) was prepared by suspending CNTs-COOH in a solution of thionyl chloride and stirring for 24 h at 70 °C. The solid was removed by filtration, washed with anhydrous THF

and dried. The so-obtained CNTs-COCl (10 mg) and completely deacetylated CS (200 mg) were added to anhydrous DMF (20 mL). The mixture was stirred at 120 °C for 96 h under a nitrogen atmosphere. After the reaction, the mixture was filtered and washed with copious amounts of 2% aqueous acetic acid solution until no CS could be detected in the filtrate. Finally, the product was dried to obtain a gray and fluffy solid (82 mg).

Oxidative Graft Polymerization of Aniline from 4-Aminothiophenol-Modified Gold Electrode. The gold electrode was immersed in a 10 mM ethanol solution of 4-aminobenzenethiol for 72 h at 35 °C to form a self-assembled monolayer (SAM) of 4-aminothiophenol. The surface was then rinsed with copious amounts of ethanol to remove the unbounded residues. The oxidative graft polymerization was carried out in 30 mL of 0.5 M aqueous solution of HCl, containing the SAM-modified gold electrode, 1 mL (~0.01 mol) of aniline and 0.23 g (~0.01 mol) of $(NH_4)_2S_2O_8$ at 0 °C for 5 h. The so-obtained electrode, referred to as the Au-*g*-PANI electrode, was washed with copious amounts of doubly distilled water and dried under reduced pressure.

Covalent Coupling of CS-CNTs onto the Au-g-PANI Electrode. Glutaraldehyde (GA) has been widely used as a cross-linking agent. In this work, GA provides the reactive aldehyde groups for covalent bonding of PANI with CS. The Au-*g*-PANI electrode was immersed in a 3% aqueous solution of glutaraldehyde under stirring at room temperature overnight. After being cleaned with copious amounts of doubly distilled water, the electrode was immersed in 10 mL of 2% aqueous solution of acetic acid containing 5 mg/mL CS-CNTs overnight. The resulting electrode was washed with doubly distilled water, dried under reduced pressure, and denoted as the Au-*g*-PANI-*c*-(CS-CNTs) electrode.

Covalent Immobilization of Glucose Oxidase (GOD) onto the Au-g-PANI-c- (CS-CNTs) Electrode. The Au-*g*-PANI-*c*-(CS-CNTs) electrode was immersed in 5 mL of dried DMSO, containing 1 g of 1,4-carbonyldiimidazole (CDI), for 24 h at room temperature, and then in a 5 mL of PBS containing 5 mg/mL of GOD for 48 h. After the immobilization reaction, the modified electrode surface was washed sequentially with excess PBS and doubly distilled water, and dried under reduced pressure.

Characterization. X-ray photoelectron spectroscopy (XPS) measurements were carried out on a Kratos AXIS HSi spectrometer equipped with a monochromatized Al Kα X-ray source (1468.6 eV photons). Field emission scanning electron microscopy (FESEM) images were obtained on a JEOL JSM-6700 scanning electron microscope. Transmission electron microscopy (TEM) images were obtained on a JEOL JEM-2010 transmission electron microscope. The electrochemical behavior and biocatalytic response of the GOD-functionalized Au electrodes to glucose were determined by cyclic voltammetry and chronamperometry measurements on an Eco Chemie Autolab PGSTAT 30 Potentiostat/Galvanostat Unit (Metrohm B.V., The Netherlands).

RESULTS AND DISCUSSION

Surface Functionalization of Au Electrodes. Panels a and b in Figure 2 show the respective X-ray photoelectron spectroscopy (XPS) wide scan and N 1s core-level spectra of the Au electrode surface with self-assembled monolayer (SAM) of 4-aminothiophenol (Au-NH_2 surface). In the wide scan spectrum, the photoelectron lines at the binding energies (BEs) of about 62, 84, 168, 285, 344, 399, and 590 eV are attributable to Au 5p, Au 4f, S 2p, C 1s, Au 4d, N 1s, and Au 4p species, respectively (38). The N 1s core-level spectrum of the Au-NH_2 surface with a BE at about 399.4 eV is attributed to the terminal amine group of 4-aminothiophenol on the Au electrode surface (38). The

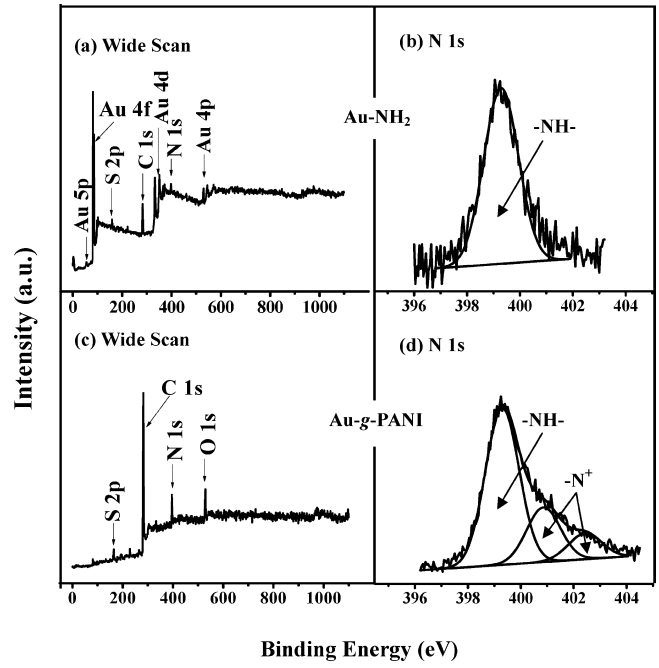

FIGURE 2. Wide scan and N 1s core-level spectra of the (a, b) Au-NH_2 surface and (c, d) Au-*g*-PANI surface.

amine functional groups on the Au surface can thus be used as anchoring sites for the subsequently oxidative graft polymerization of aniline.

Panels c and d in Figure 2 show the XPS wide scan and N 1s core-level spectra of the polyaniline (PANI)-grafted Au electrode (Au-*g*-PANI) surface. In comparison with that of the N 1s signal in the wide scan spectrum of Au-NH_2 surface in Figure 2a, the intensity of N 1s signal of the Au-*g*-PANI surface has increased significantly, whereas the Au 5p, Au 4f, Au 4d, and Au 4p signals have disappeared almost completely after the oxidative graft polymerization of aniline. The N 1s peak components with BEs at about 398.2, 399.4 and >400 eV correspond to the quinonoid imine (═N—), benzenoid amine (—NH—) and the positively charged nitrogen (N^+), respectively (39). Upon oxidative graft polymerization of aniline, the surface [C]:[N] molar ratio, as determined from C 1s and N 1s spectra area ratio, is about 6.2:1. The ratio agrees well with the theoretical [C]:[N] ratio of 6:1 for PANI, indicating successful grafting of PANI on the Au-NH_2 electrode surface.

Glutaraldehyde (GA) was used as a bifunctional linker to covalently immobilize chitosan-coupled carbon nanotubes (CS-CNTs) on the Au-*g*-PANI electrode. Figure 3a shows the XPS wide scan spectrum of the GA-coupled Au-*g*-PANI (Au-*g*-PANI-CHO) surface. In comparison with the wide scan spectra of Au-*g*-PANI surface in Figure 2c, the intensity of O 1s signal for the Au-*g*-PANI-CHO surface has increased significantly, whereas the intensity of the N 1s peak has decreased upon coupling of GA. The N 1s peak components with BEs at about 398.2, 399.4, and >400 eV correspond to the imine (═N—), amine (—NH—) and the positively charged nitrogen (N^+), respectively (Figure 3b). The appearance of a strong ═N— peak component and the decrease in —NH— peak component intensity are consistent with the reaction of O═C—H groups of GA with the -NH- groups on the Au-*g*-

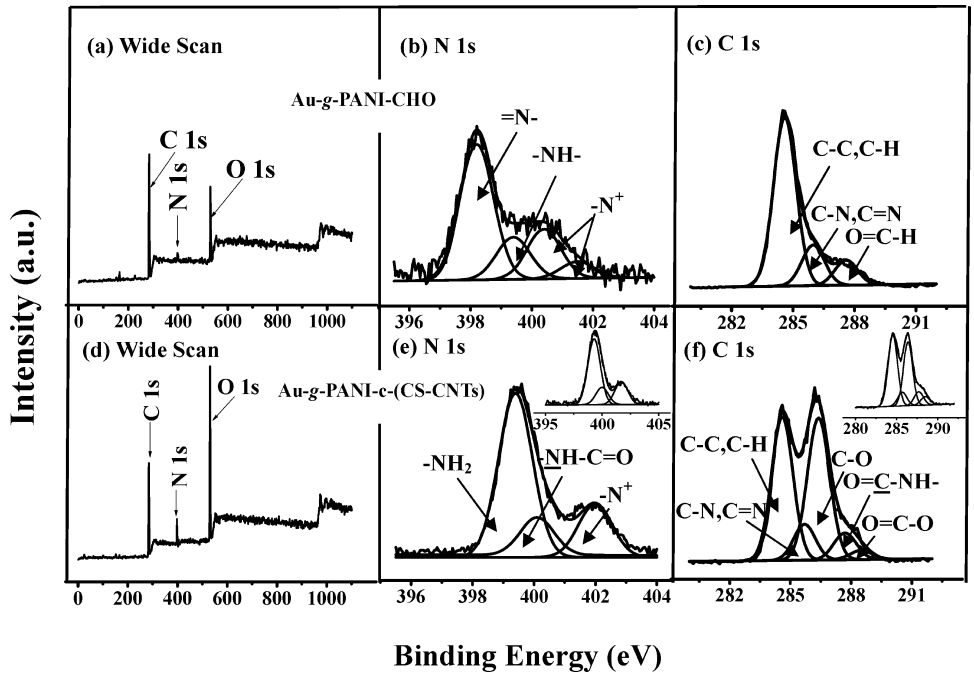

FIGURE 3. Wide scan N 1s and C 1s core-level spectra of the (a−c) Au-*g*-PANI-CHO surface, and (d−f) Au-*g*-PANI-*c*-(CS-CNTs) surface. The insets of e and f are the N 1s and C 1s core-level spectra of CS-CNTs.

PANI surface to form the C═N species. The C 1s core-level spectrum of the Au-*g*-PANI-CHO surface (Figure 3c) can be curve-fitted into three peak components with BEs at 284.6, 285.7, and 287.6 eV, attributable to the C−H, C−N/C═N, and O═C−H species, respectively (38). The results suggest that GA has been successfully coupled to the Au-*g*-PANI surface and the residual O═C−H groups can be used for the subsequently covalent coupling of CS-CNTs.

Figure 3d shows the XPS wide scan spectrum of the Au-*g*-PANI-CHO surface after coupling of CS-CNTs, or the Au-*g*-PANI-*c*-(CS-CNTs) surface. In comparison with the wide scan spectrum of the Au-*g*-PANI-CHO surface, the intensity of N 1s signal of the Au-*g*-PANI-*c*-(CS-CNTs) surface has increased significantly, arising from the contribution of the amine species in CS-CNTs. Figure 3e shows the N 1s core-level spectrum of Au-*g*-PANI-*c*-(CS-CNTs) surface. The N 1s peak components with BEs at about 399.4, 400 eV and >400 eV are attributable to $-NH_2$, −NH−C═O, and N^+ species, respectively (35). The −NH−C═O peak component is probably associated with the CS-CNTs complex arising from the reaction of the $-NH_2$ groups of CS with the O═C−Cl groups of CNTs. In comparison with the N 1s core-level spectra of the CS-CNTs (inset of Figure 3e) and Au-*g*-PANI-CHO surfaces, the disappearance of -N= species at the BE of 398.2 eV on the Au-*g*-PANI-*c*-(CS-CNTs) surface and the resemblance of the N 1s spectral line shape of Au-*g*-PANI- *c*-(CS-CNTs) to that of CS-CNTs suggest that CS-CNTs have been successfully coupled to the Au-*g*-PANI-CHO surface to a thickness greater than the probing depth of the XPS technique (~8 nm in an organic matrix (38)). The C 1s core-level spectrum of the Au-*g*-PANI-*c*-(CS-CNTs) surface (Figure 3f) can be curve-fitted into five peak components with BEs at about 284.6, 285.7, 286.2, 287.6, and 288.5 eV, attributable to the C−C/C−H, C−N/C═N, C−O, O═C−NH and O═C−O species, respectively (38). The similarity in C 1s spectral line shape of the CS-CNTs surface (inset of Figure 3f) to that of the Au-*g*-PANI-*c*-(CS-CNTs) surface further indicates that the Au-*g*-PANI-*c*-(CS-CNTs) surface is dominated by the CS-CNTs layer.

The field emission scanning electron microscopy (FESEM) images of the Au-*g*-PANI-*c*-(CS-CNTs) surface are shown in Figure 4. The nanotubes are well-dispersed on the Au-*g*-PANI-*c*-(CS-CNTs) surface (Figure 4a) to form a three-dimensional network structure on the electrode surface (Figure 4b). The three-dimensional network structure of the Au-*g*-PANI-*c*-(CS-CNTs) electrode surface provides a spatial microenvironment for enzyme incorporation, as compared to that of the planar electrode surface. The transmission electron microscopy (TEM) image in the inset of Figure 4b shows the nanostructure of the CS-CNTs. The CNTs were wrapped by the grafted CS polymer of several nanometers in thickness. The CS-CNTs exist mainly in the form of individual tubes, indicating that the coated CS layer has helped to reduce the interaction among the CNTs, thus inhibiting the aggregation of CNTs and resulting in a uniform dispersion of the coupled CS-CNTs composites on the Au-*g*-PANI-*c*-(CS-CNTs) electrode. Moreover, the uniform distribution of CS-CNTs on the Au-*g*-PANI-*c*-(CS-CNTs) electrode surface can provide a conductive pathway for electron-transfer. Thus, the present three-dimensionally coupled CS-CNTs on the Au-*g*-PANI-*c*-(CS-CNTs) electrode surface are favorable to the construction of biosensors.

The hydroxyl and amine functional groups of CS on the Au-*g*-PANI-*c*-(CS-CNTs) surface is activated by 1,4-carbonyl-diimidazole (CDI) for the subsequent immobilization of amine-containing glucose oxidase (GOD). Figure 5 shows the respective XPS C 1s and N 1s core-level spectra of the CDI-activated and GOD-immobilized Au-*g*-PANI-*c*-(CS-CNTs) sur-

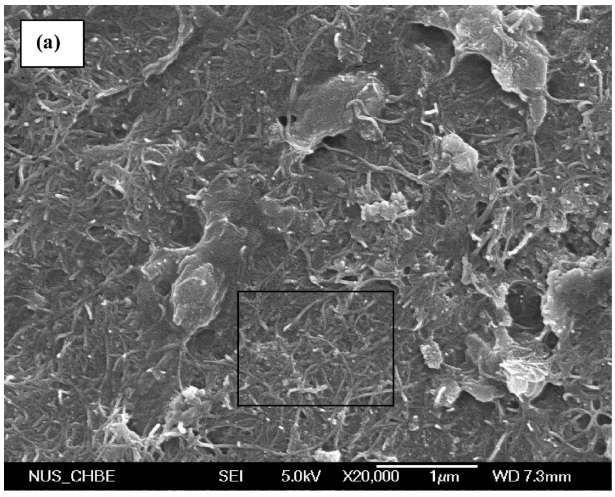

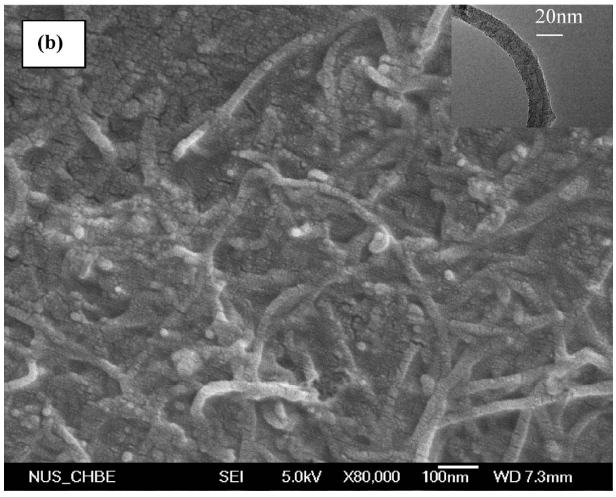

FIGURE 4. FESEM images of the Au-*g*-PANI-*c*-(CS-CNTs) surface of different magnifications.

faces (Au-*g*-PANI-*c*-(CS-CNTs)-CDI and Au-*g*-PANI-*c*-(CS-CNTs)-GOD surfaces, respectively). The C 1s core-level spectrum of the Au-*g*-PANI-*c*-(CS-CNTs)-CDI surface can be curve-fitted into five peak components with BEs at about 284.6, 285.7, 286.2, 287.6, and 288.5 eV, attributable to the C−C/C−H, C−N/C═N, C−O, O═C−NH and O═C−O species, respectively (38). The increase in O═C−O peak intensity indicates that the CDI-coupling reaction involves the reaction of the −OH groups on the Au-*g*-PANI-*c*-(CS-CNTs) surface with the carbonyl imidazole groups of CDI. The corresponding N 1s spectrum consists of the ═N− (BE∼397.9 eV), −NH− (BE∼399.4 eV), NH−C═O (BE∼400 eV) and $-N^+$ (BE > 400 eV) peak components. In comparison with the N 1s core-level spectrum of the Au-*g*-PANI-*c*-(CS-CNTs) surface, a significant increase in intensity of the ═N− peak component is associated with the coupled carbonyl imidazole groups on the Au-*g*-PANI-*c*-(CS-CNTs)-CDI surface (40). The C 1s core-level spectrum of Au-*g*-PANI-*c*-(CS-CNTs)-GOD surface (Figure 5c) can be curve-fitted into five peak components with BE values at about 284.6, 285.7, 286.2, 287.6, and 288.5 eV, attributable to the C−C/C−H, C−N/C═N, C−O, O═C−NH, and O═C−O species, respectively (38). The intensity of the O═C−NH peak component has increased significantly, arising from the contribution of the peptide bonds in GOD itself. The presence of immobilization GOD is further ascertained by the dominance of NH−C═O peak component at the BE of 400 eV in the N 1s core-level spectrum (Figure 5d). Thus, GOD has been successfully immobilized on the Au-*g*-PANI-*c*-(CS-CNTs)-CDI surface.

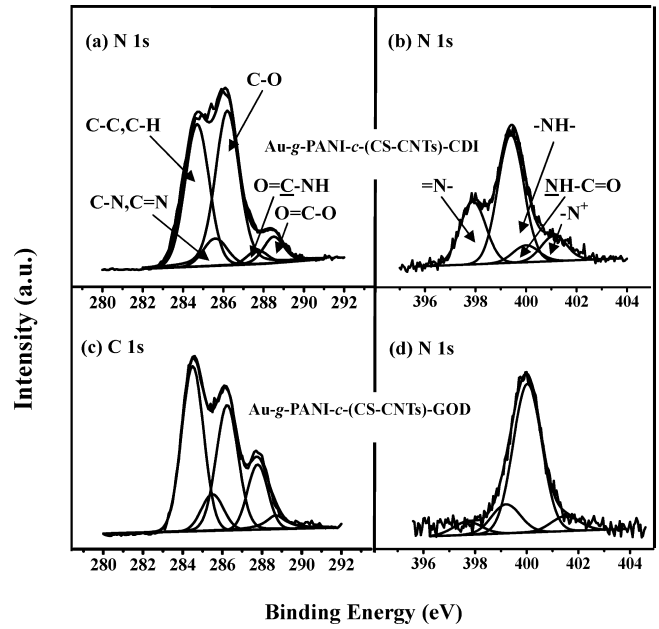

FIGURE 5. C 1s and N 1s core-level spectra of the (a, b) Au-*g*-PANI-*c*-(CS-CNTs)-CDI surface and (c, d) Au-*g*-PANI-*c*-(CS- CNTs)-GOD surface.

Electrochemical Behavior of the Au-*g*-PANI-*c*-(CS-CNTs)-GOD Electrode. The electrochemical behavior of the Au-*g*-PANI-*c*-(CS-CNTs)-GOD electrode was investigated by cyclic voltammetry (CV) using $Fe(CN)_6^{3-/4-}$ as the redox marker. Figure 6a shows the cyclic voltammograms (CVs) of the Au-*g*-PANI-*c*-(CS- CNTs)-GOD electrode recorded at different scan rates in 0.1 M phosphate buffer solution (PBS) (pH 6.0) solution containing 1 mM of $Fe(CN)_6^{3-/4-}$. The $Fe(CN)_6^{3-/4-}$ redox process is observed with an average peak separation (ΔE_p) of about 110 mV, indicating a quasi-reversible electron transfer process. For comparison purpose, an Au-*c*-(CS-CNTs)-GOD electrode without the PANI interlayer was similarly fabricated according to procedures shown in Scheme 4 of Figure 1, and studied under the same conditions. The inset of Figure 6a shows the CVs of Au-*g*-PANI-*c*-(CS-CNTs)-GOD (solid curve) and Au-*c*-(CS-CNTs)-GOD (dashed curve) electrodes recorded at scan rate of 100 mV/s. Higher cathodic and anodic peak currents are observed for the Au-*g*-PANI-*c*-(CS-CNTs)-GOD electrode, in comparison with those of the Au-*c*-(CS-CNTs)-GOD electrode. Thus, the introduction of PANI layer between the Au electrode and CS-CNTs composites enhances the redox response, indicating that the electrocatalytic activity of the electrode has been improved (41, 42), in addition to the CS-CNTs acting as mediators (43) to transfer electrons between PANI and GOD. On the other hand, the peak currents of the $Fe(CN)_6^{3-/4-}$ redox process (anodic and cathodic) of the Au-*g*-PANI-*c*-(CS-CNTs)-GOD electrode are shown to be dependent on the scan rate (Figure 6b). The anodic and cathodic

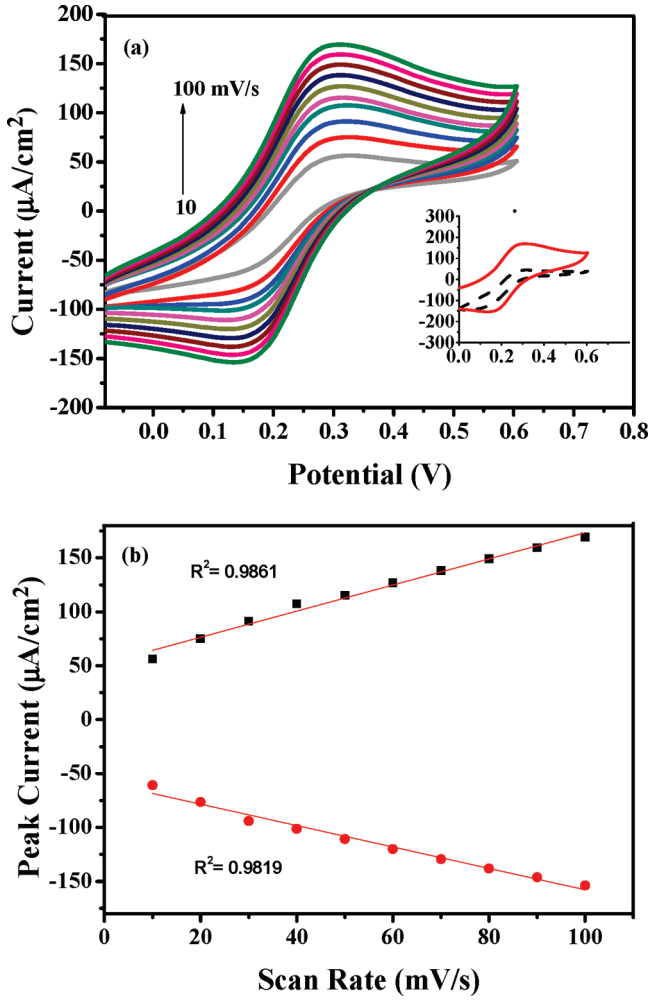

FIGURE 6. (a) Cyclic voltammograms (CVs) of the Au-*g*-PANI-*c*-(CS-CNTs)-GOD electrode at scan rates of 10, 20, 30, 40, 50, 60, 70, 80, 90, and 100 mV/s in in 1 mM PBS (pH 6.0) of $Fe(CN)_6^{3-/4-}$ under a nitrogen atmosphere. The inset is the CVs of Au-*c*-(CS-CNTs)-GOD (dash line) and Au-*g*-PANI-*c*-(CS-CNTs)-GOD (solid line) electrodes at the scan rate of 100 mV/s. (b) Dependence of peak currents on scan rates.

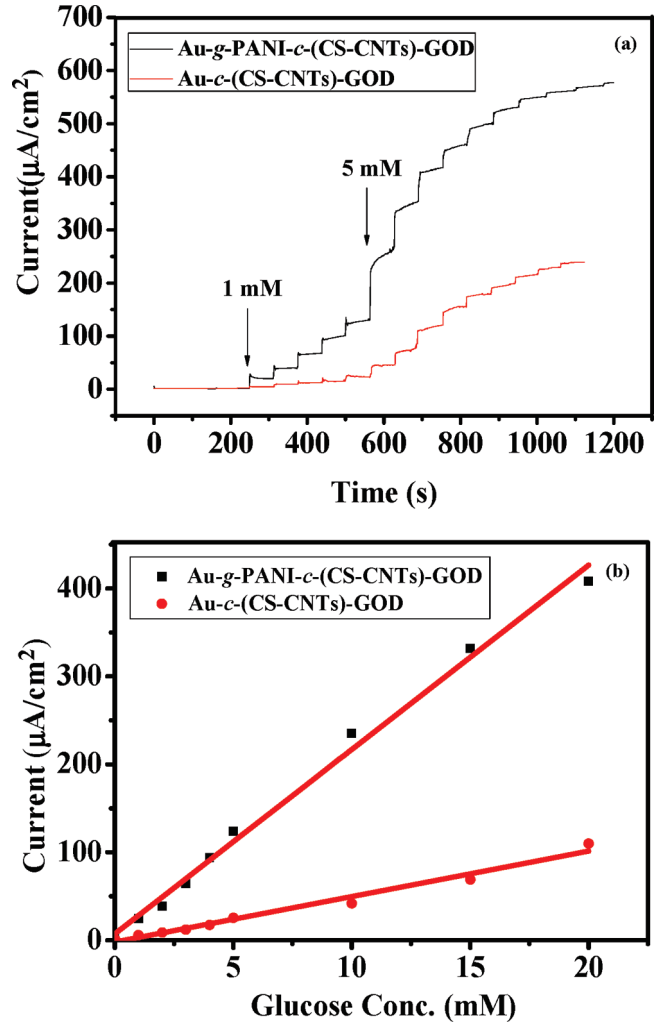

FIGURE 7. (a) Amperometric responses of the Au-*g*-PANI-*c*-(CS-CNTs)-GOD and Au-*c*-(CS-CNTs)-GOD electrodes, and (b) the linear regression analysis of the glucose concentration-current curves.

peak currents increase linearly with the scan rate, with the correlation coefficient (R^2) values of 0.9861 and 0.9819 for the anodic and cathodic peaks, respectively, in the scan rate range of 10−100 mV/s. The linearity between peak current and scan rate suggests that the redox reactions are surface-confined electrode reactions (29, 31).

Amperometric Response of the Au-*g*-PANI-*c*-(CS-CNTs)-GOD Electrode. Amperometric measurements are widely used to evaluate and analyze the performance of glucose biosensors toward an increase in glucose concentration (3, 5, 44, 45). Amperometric responses of the Au-*g*-PANI-*c*-(CS-CNTs)-GOD and Au-*c*-(CS-CNTs) -GOD electrodes were studied at a constant applied potential of 0.5 V vs the Ag/AgCl electrode. Upon each injection of glucose at regular intervals, both electrodes show a rapid and prominent increase in current, as shown in Figure 7a. The response current reaches its steady-state value within about 8−10 s at each glucose concentration and the detection limit is about 0.1 mM. This response time is comparable to that of 5−10 s for biosensors based on PANI nanofibers (14), or that of 8 s for a multicomponent biosensor (31). Furthermore, the steady-sate currents of the Au-*g*-PANI-*c*-(CS-CNTs)-GOD electrode are much larger in magnitude than those of the corresponding Au-*c*-(CS-CNTs)-GOD electrode, indicating that the sensitivity of the Au-*g*-PANI-*c*-(CS-CNTs)-GOD electrode is higher than that of the Au-*c*-(CS-CNTs)-GOD electrode. Figure 7b shows a linear relationship between the glucose concentration and the steady-state current for both electrodes at low glucose concentration. Both electrodes display a linear response in the glucose concentration range of 1 to 20 mM, which covers the expected linear range of 5−20 mM for *in vivo* monitoring (46) and is thus probably adequate for clinical applications in monitoring human glucose levels. The calculated sensitivity of the Au-*g*-PANI-*c*-(CS-CNTs)-GOD electrode form Figure 7b is about 21 μA/(mM·cm^2) (or 16.5 μA/mM), whereas that of the Au-*c*-(CS-CNTs)-GOD electrode is much lower at about 5.2 μA/(mM·cm^2) (or 4.1 μA/mM). The Au-*g*-PANI-*c*-(CS-CNTs)-GOD biosensor also exhibits higher sensitivity and wider linear response range than those reported for glucose biosensors fabricated from CS/CNTs (20, 26, 29), PANI-*g*-CS (27), and PANI-*g*-MWCNT composite (31, 47), prepared by blending (29), layer-by-layer self-assembly (20, 26, 27), electrodepo-

Table 1. Comparison of Performance of Glucose Biosensors Based on CS, CNTs, and/or PANI from Different Fabrication Methods

modified electrode[a]	linear range (mM)	sensitivity (μA/mM)	ref
GOD/CNTs/CS/GC	0−7.8	0.52	29
$(CNT/CHIT/GNP)_8/GO_x/GC$	0.006−5	3.84	26
$\{Chi/MWCNTs/GOD\}_6$	1−7	8.017	(20)
$[(CS\text{-}g\text{-}PAN/GOD)_{12}]$	1−16	~0.09	27
$\{GO_x/Au\text{-}(SH)PANI\text{-}g\text{-}MWNT\}_{10}$	1−9	3.97	31
$ITO/Nafion\text{-}silica/MWNT\text{-}g\text{-}PANI/GO_x$	1−10	5.01	47
Au-*g*-PANI-*c*-(CS-CNTs)-GOD	1−20	16.5	this work

[a] GOD, GO_x = glucose oxidase; GC = glassy electrode; CS, CHIT, Chi = chitosan; PAN, PANI = polyaniline; (SH)PAN = thio-functionalized polyaniline; NWNT, NMCNT = multiwalled carbon nanotubes; CNT = carbon nanotubes; ITO = indium−tin oxide; GNP = gold nanoparticles.

sition (31), or loading into sol−gel-derived silica (47) (Table 1). It has been reported that the increase in the amount of enzyme loading could improve the sensitivity and linear response range (48). The high surface-to-volume ratio of the three-dimensional CS-CNTs composites on the Au-*g*-PANI-*c*-(CS-CNTs)-GOD electrode has enhanced the density of GOD immobilized on the electrode, leading to an increase in biological affinity of the Au-*g*-PANI-*c*-(CS-CNTs)-GOD electrode for glucose.

The saturation in detection current can be observed for both electrodes at high glucose concentration, as shown in Figure 8a, consistent with the characteristics of the Michaelis−Menten kinetics. Figure 8b shows the Lineweaver−Burk plots of the two electrodes as a function of glucose concentration. The apparent Michaelis−Menten constant (K_m), as an indica-

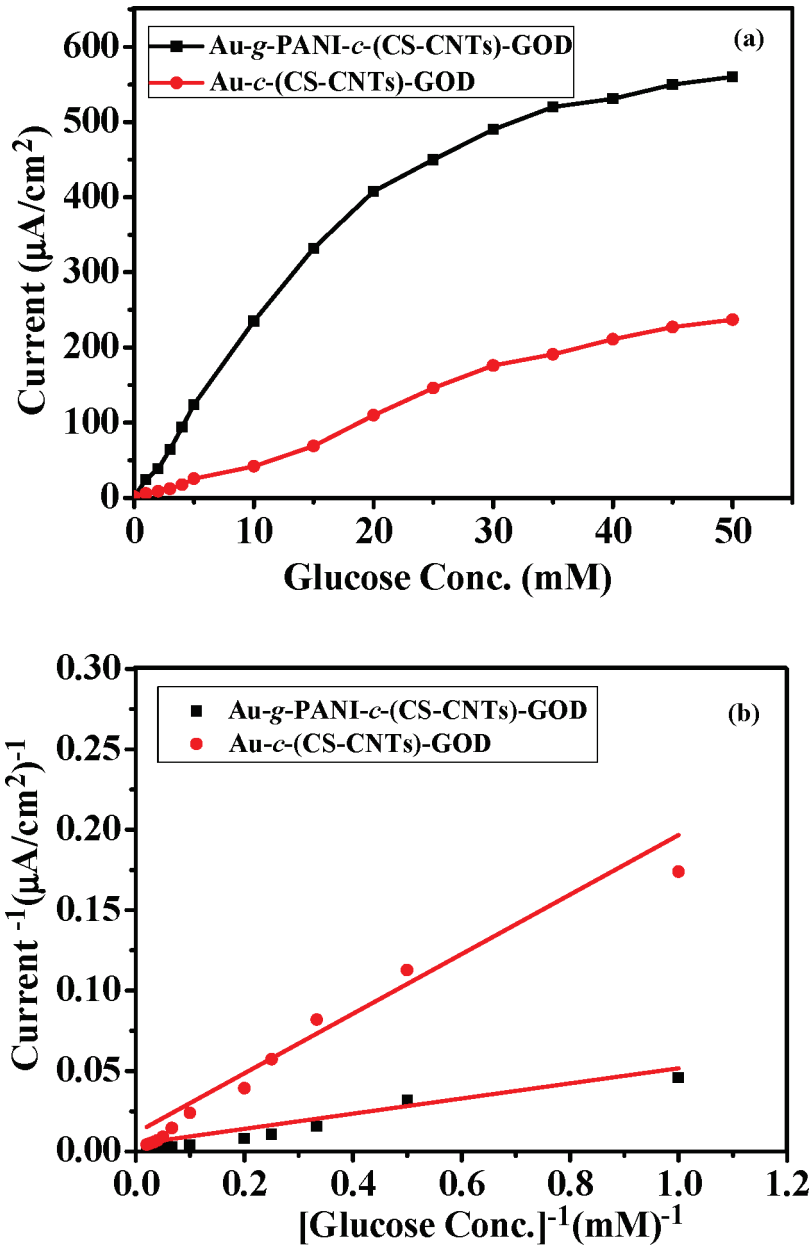

FIGURE 8. (a) Glucose concentration ($C_{glucose}$) dependence of the response current (i) for the Au-*g*-PANI-*c*-(CS-CNTs)-GOD and Au-*c*-(CS-CNTs)-GOD electrodes, and (b) the Lineweaver−Burk plots of (1)/(i_{ss}) vs (1)/($C_{glucose}$), where i_{ss} is the steady-state current.

tion of the enzyme substrate kinetics for the biosensor, can be calculated from the Lineweaver–Burk plot (49)

$$\frac{1}{i_{ss}} = \frac{K_m}{i_{max}}\frac{1}{C} + \frac{1}{i_{max}} \quad (1)$$

where i_{ss} is the steady-state current, i_{max} is the maximum current measured under saturated substrate condition, and C is the concentration of glucose. The K_m value of the Au-*g*-PANI-*c*-(CS-CNTs)-GOD electrode was obtained from the intercept and slope of the fitted curve (Figure 8b) to be 5.35 mM, which is much lower than that of the Au-*c*-(CS-CNTs)-GOD electrode (14.85 mM). Moreover, the K_m value of Au-*g*-PANI-*c*-(CS-CNTs)-GOD electrode is also lower than those reported for the GOD-CS-SiO_2/Pt/MWNTs/GC electrode (14.4 mM) (34), and GOD/CNTs/CS/GC electrode (8.2 mM) (29). The lower K_m value suggests that the immobilized GOD on Au-*g*-PANI-*c*-(CS-CNTs)-GOD electrode possesses a higher enzymatic activity (50).

Thus, the homogeneous and spatial distribution of CS-CNTs on the electrode surface has facilitated electrode-enzyme contact and contributed to the wider range of linear response. The higher sensitivity of Au-*g*-PANI-*c*-(CS-CNTs)-GOD electrode can also be attributed to the fact that the Au-*g*-PANI-*c*-(CS-CNTs)-GOD electrode has a high electrocatalytic activity, as indicated by the CV results. In addition, the processes of immobilization of PANI (51) and CS (52) probably have given rise to a more biocompatible microenvironment for improving the biological response of the enzyme.

Reproducibility and Stability of the Au-*g*-PANI-c-(CS-CNTs)-GOD Electrode. The reproducibility of current response for the Au-*g*-PANI-*c*-(CS-CNTs)-GOD biosensor was ascertained from data obtained from ten electrodes prepared under the same condition. The results reveal that the biosensor has satisfactory reproducibility with a relative standard deviation (R.S.D) of about 5.0%. The long-term stability of the Au-*g*-PANI-*c*-(CS-CNTs)-GOD biosensor was determined by storing the electrodes at 4 °C in PBS solution. The electrodes were able to maintain about 95% and 83% of the initial current response after 1 month and 2 months, respectively, of storage (Figure 9). The Au-*g*-PANI-*c*-(CS-CNTs)-GOD biosensor shows higher stability than the noncovalently (26, 53) or semicovalently (28, 47) linked biosensors, as shown in Table 2. The long-term stability of the Au-*g*-PANI-*c*-(CS-CNTs)-GOD biosensor can probably be attributed to the covalent bonding and interactions of the Au electrode with the PANI layer, CS-CNTs composites and GOD. The strong and robust covalent bonding is unaffected by changes in the surrounding environment, such as ionic strengthen, solution concentration, temperature, among others (18). Moreover, covalent bonding of GOD on the Au electrode prevents its leaching from the electrode surface during operation and storage. The electrodes were fabricated under mild conditions, with minimal damage to the enzyme molecules. The biocompatible nature of CS (20, 29, 52) and PANI (51) has helped to maintain the bioactivity of the enzyme molecules immobilized on the electrode.

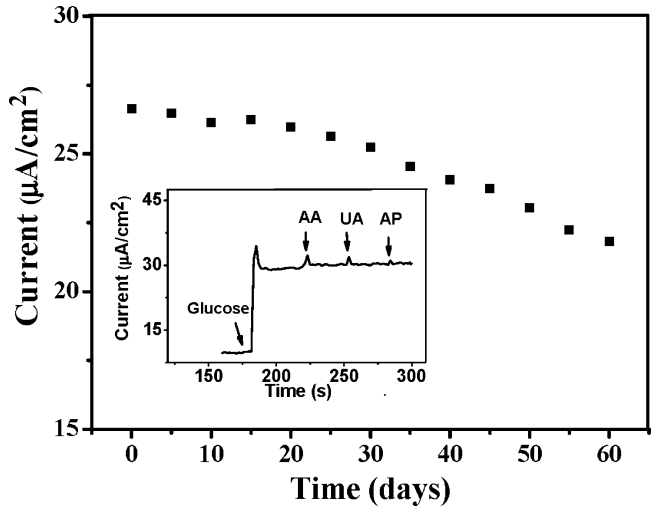

FIGURE 9. Response current ($C_{glucose}$ = 10 mM) of the Au-*g*-PANI-*c*-(CS-CNTs)-GOD electrode as a function of storage time. The inset shows the amperometric responses of the Au-*g*-PANI-*c*-(CS-CNTs)-GOD electrode to glucose (1.0 mM), in the presence of ascorbic acid (AA, 0.3 mM), uric acid (UA, 0.3 mM), and acetaminophen (AP, 0.3 mM) in PBS (pH 6.0) at an applied potential of 0.5 V.

Table 2. Comparison of Stability of Glucose Biosensors Fabricated via Non-Covalent or Semicovalent Linkage/Bonding Processes

modified electrode[a]	retention of initial current response (%)	storage time (days)	ref
GC/CNT-CHIT-GDI-GDH	80	4	28
GOD/Ag/CNT/Ch/ITO	91	10	51
$(CNT/CHIT/GNP)_8/GO_x$/GC	81.3	10	26
ITO/Nafion-silica/MWNT-*g*-PANI/GO_x	93	20	47
Au-*g*-PANI-*c*-(CS-CNTs)-GOD	97	20	this work

[a] GOD, GO_x = glucose oxidase; GDI = glutaric dialdehyde; GDH = glucose dehydrogenase; GC = glassy electrode; CS, CHIT, Ch = chitosan; PANI = polyaniline; NWNT = multiwalled carbon nanotubes, CNT = carbon nanotubes; ITO = indium–tin oxide.

The interference tests were carried out at 1.0 mM glucose concentration, with the additions of 0.3 mM ascorbic acid (AA), 0.3 mM uric acid (UA) and 0.3 mM acetaminophen (AP) at different time intervals. The normal physiological level of glucose is 3–8 mM and those of UA and AA about 0.1 mM (54). At the applied potential of 0.5 V, the response of the glucose biosensor was affected by the addition of AA and UA, as these species also yielded response current on the electrode surface. However, the high sensitivity of the biosensor toward glucose made the interferences of UA and AA acceptable (55), and that of AP negligible (inset of Figure 9).

CONCLUSIONS

An amperometric glucose biosensor has been successfully developed through covalent attachment of chitosan-carbon nanotubes (CS-CNTs) composites and glucose oxidase (GOD) on polyaniline (PANI)-modified Au electrode. The combination of PANI and CS-CNTs was shown to provide a spatially biocompatible microenvironment on the electrode surface to increase the electrocatalytic activity, better mediate the electron transfer, and enhance the activity of the

enzyme immobilized on the biosensor, thus improving its sensitivity and affinity for glucose. Moreover, the covalent immobilization process used for the fabrication of biosensors prevents GOD leaching and maintains the biological activity of GOD during operation and under storage. Therefore, the resulting biosensor exhibits high sensitivity, good reproducibility, and long-term stability. The methodology adopted in the present study provides a new platform for the fabrication of high-performance glucose and other biosensors.

REFERENCES AND NOTES

(1) Banerjee, R. R.; Rangwala, S. M.; Shapiro, J. S.; Rich, A. S.; Rhoades, B.; Qi, Y.; Wang, J.; Rajala, M. W.; Pocai, A.; Scherer, P. E.; Steppan, C. M.; Ahima, R. S.; Obici, S.; Rossetti, L.; Lazar, M. A. *Science* **2004**, *303*, 1195–1198.
(2) Wilkins, E.; Atanasov, P. *Med. Eng. Phys.* **1996**, *18*, 273–288.
(3) Yan, J.; Pedrosa, V. A.; Simonian, A. L.; Revzin, A. *ACS Appl. Mater. Interfaces* **2010**, *2*, 748–755.
(4) Wang, J. *Electroanalysis* **2001**, *13*, 983–988.
(5) Fang, B.; Gu, A. X.; Wang, G. F.; Wang, W.; Feng, Y. H.; Zhang, C. H.; Zhang, X. J. *ACS Appl. Mater. Interfaces* **2009**, *1*, 2829–2834.
(6) Trojanowicz, M.; Vel Krawczyk, T. K. *Mikrochim. Acta* **1995**, *121*, 167–181.
(7) Gerard, M.; Chaubey, A.; Malhotra, B. D. *Biosens. Bioelectron.* **2002**, *17*, 345–359.
(8) Zhang, S.; Wright, G.; Yang, Y. *Biosens. Bioelectron.* **2000**, *15*, 273–282.
(9) Guimard, N. K.; Gomez, N.; Schmidt, C. E. *Prog. Polym. Sci.* **2007**, *32*, 876–921.
(10) Ahuja, T.; Mira, I. A.; Rajesh, D. K. *Biomaterials* **2007**, *28*, 791–805.
(11) Cen, L.; Neoh, K. G.; Kang, E. T. *Biosens. Bioelectron.* **2003**, *18*, 363–74.
(12) Liu, Y. G.; Feng, X. M.; Shen, J. M.; Zhu, J. J.; Hou, W. H. *J. Phys. Chem. B* **2008**, *112*, 9237–9242.
(13) Wang, Z. Y.; Liu, S. N.; Wu, P.; Cai, C. X. *Anal. Chem.* **2009**, *81*, 1638–1645.
(14) Zhao, M.; Wu, X. M.; Cai, C. X. *J. Phys. Chem. C* **2009**, *113*, 4987–4996.
(15) Sangodkar, H.; Sukeerthi, S.; Srinivasa, R. S.; Lal, R.; Contractor, A. Q. *Anal. Chem.* **1996**, *68*, 779–783.
(16) Kazimierska, E.; Muchindu, M.; Morrin, A.; Iwuoha, E.; Smyth, M. R.; Killard, A. J. *Electroanalysis* **2009**, *21*, 595–603.
(17) Luo, Y. C.; Do, J. S. *Biosens. Bioelectron.* **2004**, *20*, 15–23.
(18) Shi, L.; Xiao, Y.; Willner, I. *Electrochem. Commun.* **2004**, *6*, 1057–1060.
(19) Krajewska, B. *Enzyme Microb. Technol.* **2004**, *35*, 126–139.
(20) Zou, Y. J.; Xiang, C. L.; Sun, L. X.; Xu, F. *Electrochim. Acta* **2008**, *53*, 4089–4095.
(21) Zhu, H. G.; Srivastava, R.; Brown, J. G.; McShane, M. J. *Bioconjugate Chem.* **2005**, *16*, 1451–1458.
(22) Kurita, K. *Prog. Polym. Sci.* **2001**, *26*, 1921–1971.
(23) Masuko, T.; Minami, A.; Iwasaki, N.; Majima, T.; Nishimura, S. I.; Lee, Y. C. *Biomacromolecules* **2005**, *6*, 880–884.
(24) Yang, S.; Tirmizi, S. A.; Burns, A.; Barney, A. A.; Risen, W. M. *Synth. Met.* **1989**, *32*, 191–200.
(25) Gao, Y.; Kyratzis, I. *Bioconjugate Chem.* **2008**, *19*, 1945–1950.
(26) Wang, Y.; Wei, W. Z.; Liu, X. Y.; Zeng, X. D. *Mater. Sci. Eng., C* **2009**, *29*, 50–54.
(27) Xu, X. H.; Ren, G. L.; Cheng, J.; Liu, Q.; Li, D. G.; Chen, Q. *J. Mater. Sci.* **2006**, *41*, 4974–4977.
(28) Zhang, M. G.; Smith, A.; Gorski, W. *Anal. Chem.* **2004**, *76*, 5045–5050.
(29) Liu, Y.; Wang, M. K.; Zhao, F.; Xu, Z. A.; Dong, S. J. *Biosens. Bioelectron.* **2005**, *21*, 984–988.
(30) Wu, Z. G.; Feng, W.; Feng, Y. Y.; Liu, Q.; Xu, X. H.; Sekino, T.; Fujii, A.; Ozaki, M. *Carbon* **2007**, *45*, 1212–1218.
(31) Komathi, S.; Gopalana, A. I.; Lee, K. P. *Biosens. Bioelectron.* **2009**, *24*, 3131–3134.
(32) Cai, C. X.; Chen, J. *Anal. Biochem.* **2004**, *332*, 75–83.
(33) Tiwari, A.; Gong, S. Q. *Electroanalysis* **2008**, *20*, 2119–2126.
(34) Zou, Y. J.; Xiang, C. L.; Sun, L. X.; Xu, F. *Biosens. Bioelectron.* **2008**, *23*, 1010–1016.
(35) Khan, R.; Dhayal, M. *Biosens. Bioelectron.* **2009**, *24*, 1700–1705.
(36) Rajesh; Bisht, V.; Takashima, W.; Kaneto, K. *Biomaterials* **2005**, *26*, 3683–3690.
(37) Rajesh; Takashima, W.; Kaneto, K. *Sens. Actuators, B* **2004**, *102*, 271–277.
(38) Wagner, C. D.; Moulder, J. F.; Davis, J. E.; Riggs, W. M. in *Handbook of X-ray Photoelectron Spectroscopy*; Perkin-Elmer: Eden Prairie, MN, 1992; pp 40, 42, 44, 60, 182.
(39) Kang, E. T.; Neoh, K. G.; Tan, K. L. *Prog. Polym. Sci.* **1998**, *23*, 277–324.
(40) Xu, F. J.; Li, H. Z.; Li, J.; Eric Teo, Y. H.; Zhu, C. X.; Kang, E. T.; Neoh, K. G. *Biosens. Bioelectron.* **2008**, *24*, 773–780.
(41) Teles, F. R. R.; Fonseca, L. P. *Mater. Sci. Eng., C* **2008**, *28*, 1530–1543.
(42) Sarma, A. K.; Vatsyayan, P.; Goswami, P.; Minteer, S. D. *Biosens. Bioelectron.* **2009**, *24*, 2313–2322.
(43) Liu, X.; Neoh, K. G.; Kang, E. T. *Biosens. Bioelectron.* **2004**, *19*, 823–834.
(44) Emr, S. A.; Yucynych, A. M. *Electroanalysis* **1995**, *7*, 913–923.
(45) Garjonyte, R.; Malinauskas, A. *Biosens. Bioelectron.* **2000**, *15*, 445–451.
(46) Reach, G.; Wilson, G. S. *Anal. Chem.* **1992**, *64*, 381A–386A.
(47) Gopalan, A. I.; Lee, K. P.; Ragupathy, D.; Lee, S. H.; Lee, J. W. *Biomaterials* **2009**, *30*, 5999–6005.
(48) Yang, M. H.; Qu, F. L.; Lu, Y. S.; He, Y. G.; Shen, L.; Yu, R. Q. *Biomaterials* **2006**, *27*, 5944–5950.
(49) Kamin, R. A.; Wilson, G. S. *Anal. Chem.* **1980**, *52*, 1198–1205.
(50) Zhang, S. X.; Wang, N.; Yu, H. J.; Niu, Y. M.; Sun, C. Q. *Bioelectrochemistry* **2005**, *67*, 15–22.
(51) Kamalesh, S.; Tan, P. C.; Wang, J. J.; Lee, T.; Kang, E. T.; Wang, C. H. *J. Biomed. Mater. Res.* **2000**, *52*, 467–478.
(52) Chua, P. H.; Neoh, K. G.; Kang, E. T.; Wang, W. *Biomaterials* **2008**, *29*, 1412–1421.
(53) Lin, J. H.; He, C. Y.; Zhao, Y.; Zhang, S. S. *Sens. Actuators, B* **2009**, *137*, 768–773.
(54) Wang, W.; Zhang, L. L.; Tong, S. F.; Li, X.; Song, W. B. *Biosens. Bioelectron.* **2009**, *25*, 708–716.
(55) Wang, H. C.; Wang, X. S.; Zhang, X. Q.; Qin, X.; Zhao, Z. X.; Miao, Z. Y.; Huang, N.; Chen, Q. *Biosens. Bioelectron.* **2009**, *25*, 142–146.

AM100591T